RESEARCH ARTICLE

Asian Research Association

INTERNATIONAL RESEARCH JOURNAL OF MULTIDISCIPLINARY TECHNOVATION

DOI: 10.54392/irjmt2344

# Antimicrobial activity of Cobalt doped Cerium Oxide (Co-$CeO_2$) nanoparticles against selected food pathogens

**C. Kumaran [1], I. Baskaran [2,*], K. Vanmathi Selvi [3], C. Senthamil Selvi [4], P. Rajkumar [5], S. Selvaraj [6,*]**

[1] Department of Physics, Sri Akilandeswari Women's College, Wandiwash-604408, Tamil Nadu, India
[2] Department of Physics, Arignar Anna Government Arts College, Cheyyar-604407, Tamil Nadu, India
[3] Department of Microbiology, Sri Akilandeswari Women's College, Wandiwash-604408, Tamil Nadu, India
[4] Department of Physics, S. A. Engineering College, Chennai-600077, Tamil Nadu, India
[5] PG Department of Physics, King Nandhivarman College of Arts and Science, Thellar-604406, Tamil Nadu, India, Affiliated to Thiruvalluvar University, Serkkadu, Vellore-632115, Tamil Nadu, India
[6] Department of Physics, Saveetha School of Engineering, Saveetha Institute of Medical and Technical Sciences (SIMATS), Thandalam, Chennai-602105, Tamil Nadu, India
*Corresponding author's email: ibk1978@gmail.com (I. Baskaran), sselvaphy@gmail.com (S. Selvaraj)
DOI: https://doi.org/10.54392/irjmt2344
Received: 10-05-2023; Revised: 30-06-2023; Accepted: 04-07-2023; Published: 25-07-2023

**Abstract:** This present work is to investigate the antibacterial activity of $CeO_2$ nanoparticles on five foodborne pathogens. Low-temperature solid-state reactions were used to create co-doped $CeO_2$ nanoparticles (Co-$CeO_2$ NPs). In the current work, the impact of Co-doping on polycrystalline $CeO_2$ samples synthesized using the co-precipitation method at room temperature for Co-doping concentrations of 0.5%, 1%, 3%, and 5% is discussed. Rietveld refinement of the X-ray diffraction patterns confirms that the Co-doped $CeO_2$ samples have a face-centred cubic structure. This shows that the Co ions have been successfully integrated into the $CeO_2$ lattice. Also, the UV-Vis-NIR absorption spectra confirm that redshifts do happen in the Co-doped $CeO_2$ samples, which shows that the band gap energy decreases as the number of Co ions grows. In an antibacterial test against five pathogenic microbes, S. aureus, M. luteus, Enterobacter aerogenes, S. typhi, and Pseudomonas aeruginosa, Co-doped cerium oxide nanoparticles significantly slowed the growth of all five pathogens, both in liquid and solid growth conditions. These results show that Co-doped $CeO_2$ nanoparticles have strong antibacterial properties against foodborne pathogens. This suggests that they could be used as promising bionanomaterials for in vivo therapeutic uses.

**Keywords:** Foodborne pathogens, Cobalt doped cerium oxide, Antibacterial activity, Spherical Nanoparticles

## 1. Introduction

The potential for developing nanomaterials with increased reactivity and unique properties based on their form and size is addressed by the growing area of nanoscience. It is commonly acknowledged and known that nanotechnology has had a profound impact on human existence. Understanding the nanoscale phenomena of materials necessitates the creation of nanoparticles with improved control over their size and shape, as well as the characterization of their properties, data analysis, and theoretical justifications. Nanotechnology has the potential to revolutionize many industries, including electronics, material science, biology and medicine, the environment, and information technology [1, 2]. According to the European Commission (2011/696/EU), a material made up of particles that exist in an unbound state, as an aggregation, or as an agglomeration, with at least 50% of the particles having one or more exterior dimensions in the range of 1-100 nm, is categorized as a nanomaterial. Due to their small size and high surface area-to-volume ratio, these nanoparticles have distinctive surface characteristics and heightened reactivity [3].

Metal oxides are crucial to several fields of chemistry, physics, and material science [4]. Because of their small size and many angle or edge surface atoms, oxide nanoparticles can display rare physical and chemical features. The numerous uses of cerium oxide in the fields of catalysis, electrochemistry, photochemistry, and material science make it a necessary component of this group. Since it has an empty 4f electronic structure, nanophase cerium oxide (nanoceria) is a particularly intriguing substance that can shield electrons from an oxidizing or reducing environment. Nanoceria contains a significant amount of oxygen vacancy defects compared to bulk cerium oxide,

which will enhance the material's performance. Drug-resistant pathogenic organisms that cause infectious diseases are the main cause of the growing usage of nanomedicine, an emerging field of nanotechnology. As a result of their distinctive physical and chemical characteristics, metal nanoparticles have tired the interest of numerous scholars over the years for their potential use in a variety of biological applications [5]. $CeO_2$, an extensively utilized rare earth element in nanoparticle applications, has demonstrated promising antibacterial properties and is produced through a variety of methods. The ability of $CeO_2$ nanoparticles to scavenge reactive oxygen species (ROS) and their antibacterial activity against both Gram-positive and Gram-negative bacteria [6] have sparked a growing interest in their use in medicine. Its ability to transition between the reduced and oxidized states is one of $CeO_2$'s distinguishing characteristics, setting it apart from other nanoparticles of metal oxide. In this investigation, the antibacterial activity of cobalt-doped $CeO_2$ nanoparticles against foodborne pathogens was investigated. Using the agar well diffusion method and minimum inhibitory concentrations (MICs), the antibacterial efficacy of the nanoparticles was evaluated.

## 2. Materials and Methods

### 2.1 Synthesis of Cobalt Doped Cerium Oxide NPs

$Co(NO_3)_2.6H_2O$ (50mM) and $Ce(NO_3)_2.6H_2O$ were uniformly ground before being combined and dissolved in 100 ml of distilled water while being continuously magnetically stirred. A quantifiable amount of polyethene glycol (PEG) was injected, 4 ml at a 10% concentration, to stop the polymerization process. The combination was then treated with NaOH solution to bring the pH level up to 11. The finished product was dried at 100°C in a hot air oven and then calcined at 300°C for three hours after going through many cycles of washing and filtering with distilled water. The formula $Co_{1-x}Ce_xO$ was used to express the different compositions of the cobalt substituted samples, where x was one of the following values: 0, 0.5, 1, 3, or 5.0 moles (%).

### 2.2. Characterization

X-ray diffractometer (XRD, Shimadzu6000) analysis was used to determine the crystallinity of the synthesised nanoparticles. A spectrophotometer (UV-visible, Jasco V530) was used to examine the nanoparticles' absorption properties. Measurements were made using a spectro-fluorometer (Horiba Jobin, Flouromax-4) to examine the emission spectra of the nanoparticles. The research was done using a scanning electron microscope (SEM, JOEL JSM-6390) to examine the surface morphology of the nanoparticles and comprehend how they grow to different sizes.

### 2.3. Isolation of Foodborne pathogens

The foodborne pathogens were isolated from ruined food components. Small vegetable samples ranged in size from 300 to 500 g, and all samples were kept in storage at 4°C for microbiological assays to be performed within 24 hours of sample collection**.**

### 2.4. Morphological Characterization

Microscopical techniques were used to characterize morphological features. The organism was identified by comparing the observed structure to Bergey's Manual of Determinative Bacteriology, ninth edition, published in 2000. The foodborne material was incubated at 37°C for 24 hours after being inoculated on a variety of agar plates, including nutrition agar, blood agar, pseudomonas isolation agar, Mannitol salt agar, XLD agar, and EMB agar. The colonies' colony morphology, including colour, growth pattern, and type, were then documented while being scrutinized under a strong microscope. Standard microbiological techniques were used for the characterization of bacterial isolates. Colony morphology, motility, the catalase, oxidase, and coagulase tests, as well as biochemical tests like the Triple Sugar Iron Agar, Hydrogen Sulphide, Carbohydrate Fermentation, Phenylalanine Deaminase, Methyl Red, Nitrate Reduction, Urease, Voges Proskauer, Citrate Utilization, and Indole tests, were used to identify isolates.

### 2.5. Antibacterial activity

#### 2.5.1. Disc Diffusion method

The disc diffusion method was used to assess the antibacterial activity of both pure cerium oxide and cobalt-doped cerium oxide nanoparticles against foodborne pathogens. For both pure $CeO_2$ and Co-doped $CeO_2$, a suitable concentration of 1 mg/ml dimethyl sulfoxide solution was utilized to create the nanoparticles for this approach. The dispersed nanoparticles were then injected into each sterile disc using a micro-pipette. The discs were then sterilized, put on Mueller Hinton Agar medium with a culture switch, and incubated for 24 hours. The typical zone of inhibition's diameter was expressed in millimetres (mm).

#### 2.5.2. Minimum Inhibitory Concentration (MIC):

Co-doped $CeO_2$ nanoparticles' MIC (Minimum Inhibitory Concentration) was calculated in a 96-well microplate using the broth microdilution technique. The pathogens were cultured on MHB (Mueller Hinton Broth) overnight at 37°C and adjusted with 0.5 McFarland standards to reach a final density of 1 × 108 CFU/mL. Co-doped $CeO_2$ nanoparticles were dissolved in DMSO at a 1 mg/mL concentration, and doubling dilutions were made to get concentrations ranging from 7.8 to 500 g/mL. 90 mL of MH broth, 10 mL of culture medium, and

10 mL of co-doped $CeO_2$ nanoparticles at various concentrations were introduced to each well of the microtiter plate. After that, the microtiter plate was incubated for 18 hours at 37 degrees Celsius. Following incubation, turbidity was determined using a microplate reader (Synergy HT, BioTek, USA) operating at 550 nm. The lowest concentration of Co-doped $CeO_2$ nanoparticles that caused no turbidity in the wells was chosen as the MIC value. The MIC tests were carried out three times to ensure accuracy and to catch any mistakes.

#### 2.5.3. Minimum Bactericidal Concentration (MBC):

By adding 10 l of suspension to each well of the microtiter plate used to compute the bacteria's MIC and incubating it at 37 °C for 24 hours, the minimum bactericidal concentration (MBC) was ascertained. The lack of colonies on the agar dishes served as the basis for choosing the NPs concentration that had a bactericidal effect. A negative subculture or the appearance of just one colony following incubation were examples of MBC.

## 3. Results and Discussion

### 3.1. Synthesis and Characterization of Cobalt doped Cerium Oxide NPs

In this study, we have synthesized $Co_{1-x}Ce_xO$ with x being 0, 0.5, 1.0, 3.0 and 5.0 mole (%) samples using the co-precipitation method at room temperature. A vibrating sample magnetometer (VSM), X-ray diffraction (XRD), UV-Vis-NIR optical absorption spectroscopy, and DC magnetization have all been used to examine the structural, optical, magnetic, and electronic properties in diverse investigations.

### 3.2. XRD analysis

The indexed powder XRD patterns of $Co_{1-x}Ce_xO$ are shown in Figure. (1), where x is the mole fraction of the polycrystalline samples (0, 0.5, 1.0, 3.0, and 5.0). The face-centred cubic fluorite structure of $CeO_2$ is consistent with the measured Miller indices (111), (200), (220), (311), (222), (400), and other discovered Bragg peaks in the XRD patterns. In the Co-doped $CeO_2$ samples, it is noteworthy that there are no unindexed peaks associated with secondary phases like CoO, $Co_2O_3$, or $Co_3O_4$, proving the single-phase nature of $Co_{1-x}Ce_xO$ for all x values (0, 0.5, 1.0, 3.0, and 5.0 mole%).

It's interesting to note that co-doping has affected the intensity peaks of $CeO_2$, with observable changes in the peak's intensity for various doping levels. In particular, the intensity peak for 5% Co-doped $CeO_2$ is greater, but the intensity peak for the 5% Co-doped $CeO_2$ sample is smaller [7-9]. The peak's declining intensity shows that Ce ions are moving from $Ce^{4+}$ sites to interstitial sites as a result of the sub-situation of $Co^{2+}$ or $Co^{3+}$ ions, which is also to blame for the plane's declining atomic concentration. We acquired a clear and improved viewpoint on the changing peaks by restricting the 2 range at the strongest Bragg reflection (111), displaying the diffraction pattern, and referring to Fig. 1. The plot shows that increasing Co-doping, from 0.5% to 5%, causes the Bragg peaks to shift towards higher angles. This finding provides additional proof that the Co ions were successfully incorporated into the $CeO_2$ matrix. The difference in ionic radii between the host cation $Co^{2+}$ (0.72 Å) and host cation $Ce^{4+}$ (0.92 Å) ions, as well as the intensity of all diffraction peaks in the XRD patterns, are also responsible for this rise. With the rise in dopant concentration, this change in radii also affects the crystallization of $CeO_2$.

### 3.3. UV Spectra

To examine the optical characteristics of the synthesized Co-doped and pure $CeO_2$ nanoparticles, the UV-visible spectrophotometer was used. Figure. 2(b) shows the UV-visible absorption spectra of both the pure and Co-doped $CeO_2$ nanoparticles, which both exhibit a strong absorption peak at 312 nm. Pure and Co-doped cerium oxide nanoparticles' positioning of the absorption peaks points to their fluorite cubic structure [10]. The Kubulka-Munk function is used to determine the estimated band gap of the synthesized nanoparticles, where $E_g$ is the direct band gap energy [11]. Figure. 2(a) depicts the graph of $(\alpha h\nu)^2$ versus energy that has been made. The straight portion of the curve was extrapolated to the energy axis to produce the band gap energies. In Fig.2(a), the calculated energy of the direct band gaps of Co-doped and pure $CeO_2$ nanoparticles are indicated [12]. As compared to undoped $CeO_2$ nanoparticles ($E_g$ = 3.15eV), it has been found that the band gap ($E_g$) of Co-doped $CeO_2$ nanoparticles has dramatically moved (3.15 eV, 3.104 eV and 2.964 eV for $Co_{0.00}$ $Ce_{100}O_2$, $Co_{0.3}Ce_{99.7}O_2$ and $Co_{0.5}Ce_{99.5}O_2$, respectively). When compared to the values listed in published literature, the observed movement is noticeably less after two or three valence cobalt ions are substituted for cerium ions in the $CeO_2$ matrix to maintain charge neutrality [13].

### 3.4. Magnetic behaviour

Figure. 3 shows the hysteresis curve of cobalt-doped and pure cerium oxide nanoparticles. Surprisingly, the synthesized nanoparticles exhibit room-temperature ferromagnetism (RTFM). The exact values of saturation magnetization (Ms), coercive field (Hc), and magnetic remanence (Mr) for each sample are shown in Table 1. According to the M-H loop analysis, the presence of Co in the host matrix causes an increase in Ms and a decrease in the Hc and Mr values of $CeO_2$ nanoparticles. Unexpectedly, pure $CeO_2$ nanoparticles showed RTFM, surpassing previously reported values for magnetization and coercivity for pure $CeO_2$ [14] with

a Ms value of 0.00283 emu/g. The RTFM behaviour of $CeO_2$ has also been documented by several other research teams [15-17]. The precise mechanism causing RTFM to start in rare earth metal oxides is not entirely understood, though. It has been proposed that interactions between electron spin moments caused by oxygen vacancies (Vo) at the particle surface may be the source of the ferromagnetic behaviour in $CeO_2$ nanostructures. Cobalt-doped $CeO_2$ nanoparticles exhibit room-temperature ferromagnetism (RTFM), which can be explained via F-center exchange (FCE) coupling, as has been shown by numerous research teams [18]. When an electron in an oxygen vacancy (Vo) is trapped by the FCE procedure, an F-center is created. Two Co ions combine to produce Co-Vo-Co groups when Vo is present. The trapped electron in Vo also eliminates the orbital overlap with the nearby Co ions. The spins of the trapped electrons should align parallel to the spins of the two closest Co ions by Pauli's exclusion principle and Hund's rule, resulting in the establishment of ferromagnetic (FM) ordering. It is common knowledge that $CeO_2$ has a propensity to produce oxygen vacancies at the nanoscale, making it a viable medium for storing oxygen. To preserve charge neutrality, the divalent or trivalent Co doping ions also enhance the amount of Vo in the doped $CeO_2$ nanoparticles [19].

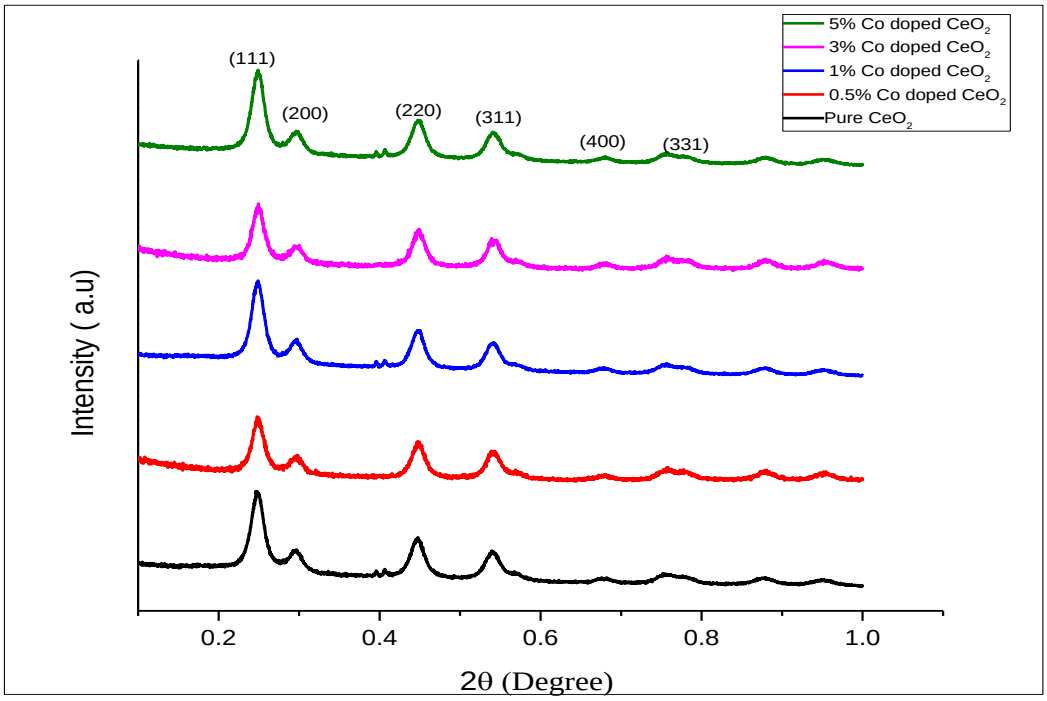


**Figure 1.** XRD patterns of the prepared samples and & Co loading induced shift in the (111) plane

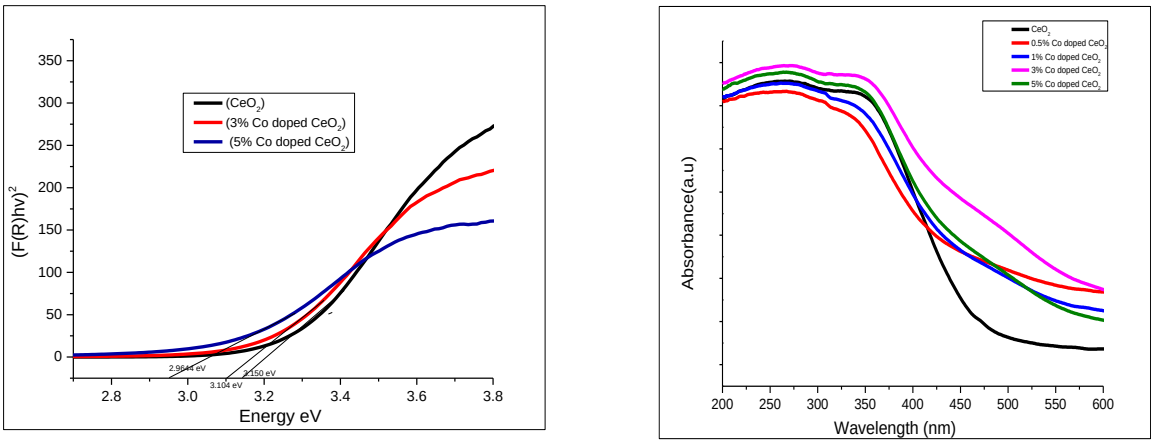


**Figure 2(a) & 2(b)** UV-visible absorption spectra of the undoped and Co-doped $CeO_2$ nanoparticles

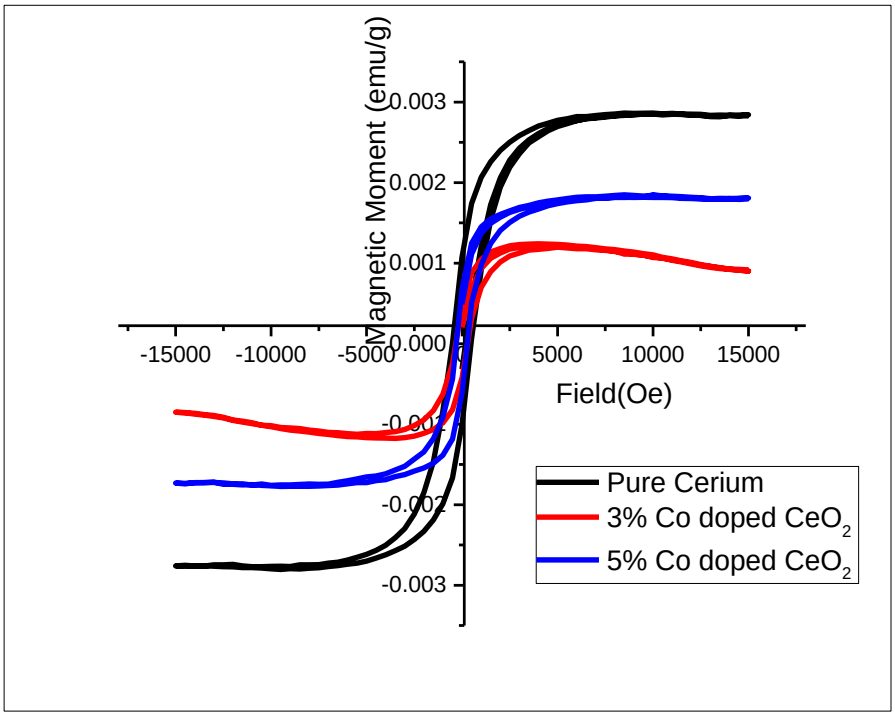


**Figure 3.** M-H loops of undoped and Co-doped $CeO_2$ nanoparticles (Inset of the figure shows opened loops)

**Table 1.** Magnetic Properties of Pure CeO2 and Doped with Co (3 % & 5 %)

| **Magnetic Properties** | **Pure $CeO_2$** | **3% Co doped $CeO_2$** | **5% Co doped $CeO_2$** |
|---|---|---|---|
| Coercivity (Hci) | 486.37 Oe | 307.83 Oe | 287.17 Oe |
| Field Increment | 500 Oe | 500 Oe | 500 Oe |
| Magnetization (Ms) | 2.8342 x $10^{-3}$ emu | 1.2082 x $10^{-3}$ emu | 1.8106 x $10^{-3}$ emu |
| Mass | 27 x $10^{-3}$ g | 21 x $10^{-3}$ g | 13 x $10^{-3}$ g |
| Number of Points | 151 | 151 | 151 |
| Retentivity (Mr) | 1.0347 x $10^{-3}$ emu | 450.02 x $10^{-6}$ emu | 640.17 x $10^{-6}$ emu |
| Sensitivity | -6.7000 emu | -6.6000 emu | -6.6000 emu |

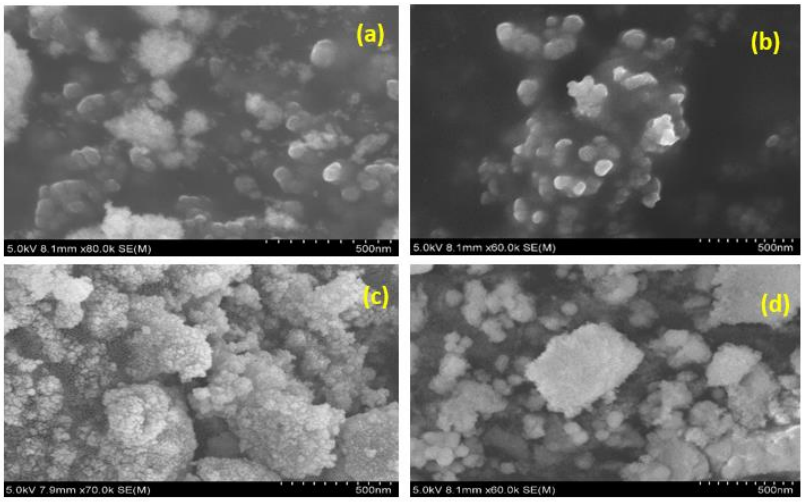


**Figure 4.** SEM images of $Co_{1-x}Ce_xO_2$ nanoparticles. (a) undoped $CeO_2$, (b) 1% Co doped $CeO_2$, (c) 3% Co doped $CeO_2$, (d) 5% Co doped $CeO_2$

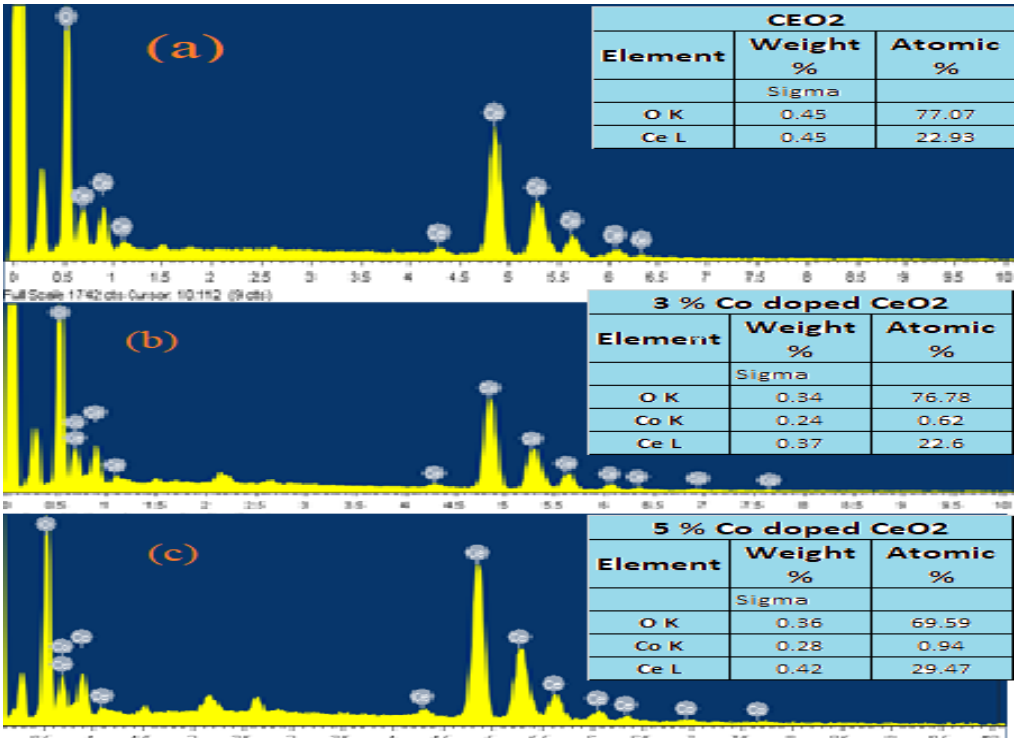


**Figure 5 (a,b,c)** EDAX spectra of (a) pure $CeO_2$and (b) 3% Co doped $CeO_2$ NPs (c) 5% Co doped $CeO_2$NPs

Because it indicates a magnetic phase transition towards super-paramagnetic behaviour in the synthesised Co-doped $CeO_2$ nanoparticles, the drop in coercive field (Hc) values brought on by Co doping is important. Super-paramagnetism can be shown in nanoparticles with incredibly small crystallite sizes thanks to structural investigations, and ZnO nanostructures doped with transition metals have also shown similar results [20].

### 3.5. SEM-Co-$CeO_2$

Both undoped and co-doped $CeO_2$ samples' scanning electron microscopy (SEM) pictures are clearly shown in Figure 4, exhibiting their different zero-dimensional (0-D) nanostructures. It is clear from all of the micrographs that the nanoparticles have a remarkably uniform size distribution and spherical shape. It has been discovered that the interaction of the Co and Ce cations, with their various valence states, ionic radii, and Pauling electronegativities, greatly affects the particle size of the generated nanoparticles, which ranges from 10 to 40 nm.

### 3.6. EDAX-Co-$CeO_2$

As shown in Fig. 5 (a, b, and c), the EDAX spectrum gave elemental mapping of the samples, including both pure and Co (3% and 5%) doped $CeO_2$ nanoparticles. The distribution of the elements Ce, Co, and O throughout the sample fits the predicted stoichiometry, according to the inset graph in the picture. With oxygen (O), cerium (Ce), and cobalt (Co) showing the largest peaks across all samples, the constituent elemental quantities and ratios are consistent with the anticipated elemental distribution. The elemental weight proportion percentages are further illustrated in the weight and atomic percentage tables.

It is clear from looking at the SEM cross-sectional images of the pure and Co (0%, 3%, and 5%) doped $CeO_2$ nanoparticles in Fig. 5 (a-c) that the aggregation of spherical-shaped nanoparticles grows as the cobalt concentration in cerium oxide increases while maintaining a narrow size distribution.

### 3.7. Isolation and Identification

The antibacterial effectiveness of cerium oxide nanoparticles, which were extracted from damaged foods like vegetables, is tested using different bacterial strains. Morphologically and biochemically, the isolated bacteria were recognized as S. aureus, M. luteus, Enterobacter aerogenes, S. typhi, and Pseudomonas aeruginosa. Isolates were not identified using the selective medium. However, isolates were streaked in distinct selective media (gramme negative in nutrition agar and Mac Conkey agar, gramme positive in Blood agar) for further analysis.

**Table 2.** Antibacterial activity of Co-doped CeO2 Nps at 50µg/mL and Ciprofloxacin 10µg/mL, against Foodborne pathogens

| S.No | Bacterial Isolates | CO-doped CeO2 NPS Zone of Inhibition (mm Diameter) | Ciprofloxacin Zone of Inhibition (mm Diameter) |
|---|---|---|---|
| 1 | *Staphylococcus aureus* | 10± 0.05 | 16± 0.02 |
| 2 | *Micrococcus luteus* | 11± 0.02 | 18± 0.01 |
| 3 | *Enterobacter aerogenes* | 8± 0.02 | 14± 0.05 |
| 4 | *Salmonella typhi* | 7± 0.03 | 17± 0.04 |
| 5 | *Pseudomonas aeruginosa* | 9± 0.05 | 15± 0.01 |

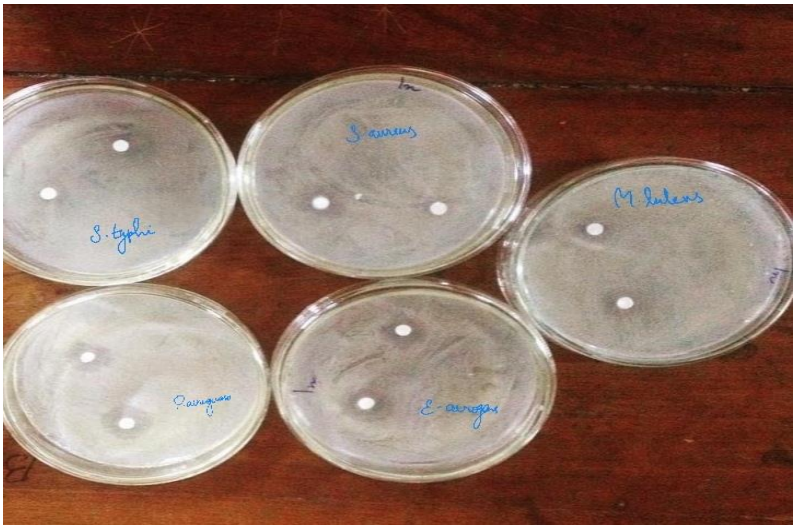


**Figure 6.** Disc diffusion assay of Cobalt doped Cerium oxide Nanoparticles

**Table 3.** Minimum Inhibitory Concentration (MIC) of Co-doped $CeO_2$ Nps & Ciprofloxacin against Foodborne pathogens

| S.NO | Bacterial Isolates | Co-doped CeO2 Nps MIC (mg/mL) | Ciprofloxacin MIC (mg/mL) |
|---|---|---|---|
| 1 | *Staphylococcus aureus* | 5 | 0.75 |
| 2 | *Micrococcus luteus* | 1.05 | 0.97 |
| 3 | *Enterobacter aerogenes* | 3.16 | 3.12 |
| 4 | *Salmonella typhi* | 2.08 | 0.56 |
| 5 | *Pseudomonas aeruginosa* | 4.51 | 0.35 |

### 3.8. Antibacterial Assay of Co-Doped Cerium Oxide Nanoparticles

Table 2 displays the Co-doped $CeO_2$NPs' antibacterial performance. The zone of inhibition (ZOI) is greater in the co-doped $CeO_2$NPs. The antibacterial properties of the NPS produced in this investigation are comparable to those reported in earlier studies [21-23], showing the effectiveness of the particles to fight multi-drug-resistant germs in the environment in a variety of applications.

The microdilution method was used to assess $CeO_2$ NP's antibacterial properties. The cobalt-doped cerium oxide nanoparticles' antibacterial efficacy was assessed against five bacterial food pathogens. By

using the broth dilution method, it was discovered that all of the isolated strains were susceptible to the Co-doped $CeO_2$ nanoparticles.

The goal of the study was to establish CeNP's MIC against diverse Gram-positive and Gram-negative bacteria [24]. Haemophilus influenzae (Gram-negative) ATCC 29247 (360 ±160 g/mL and 530± 0.0 µg/mL); Staphylococcus epidermidis (Gram-positive) ATCC 12228 (µg/mL and 90 ± 40 µg/mL); Enterobacter aerogenes (Gram-positive) ATCC 19615 (µg/mL and g/mL);

The lowest concentration that precluded observable growth was determined to be the MIC. By subculturing 250 g/ml onto PCA plates from each negative test tube, the MBC was ascertained. MBC was defined as the concentration at which there was either no subculture or just one colony present following incubation. Each pathogen underwent two replication of the experiments. It is only partially understood how cerium oxide nanoparticles hinder the growth of bacteria. Cerium oxide nanoparticles are associated with the thiol groups in the cell wall, which causes reactive oxygen species to be produced and disrupts the cell [25-26]. Cerium oxide nanoparticles are intimately associated with the bacterial cell wall, generating "pits" that eventually disrupt permeability and result in cell death [27-30]. The size of the cerium oxide nanoparticles allowed them to enter the bacterial cell easily and have an impact on intracellular processes like DNA, RNA and protein synthesis. Depending on the surface area available for the interaction, cerium oxide nanoparticles were interacting with bacteria. Smaller nanoparticles have a greater bactericidal effect than larger ones because they touch the bacteria's larger surface area [31-33].

## 4. Conclusion

Using the low-temperature solid-state reaction method, cobalt-doped cerium oxide nanoparticles were successfully synthesised. The Surface Plasmon Resonance (SPR) feature of the synthesised nanoparticles was investigated using UV-Vis spectroscopy, and the spectra showed a peak at 420-440 nm. The cerium oxide nanoparticles' spherical shape and diameter range of 45 nm to 70 nm were discovered through morphological investigation utilising scanning electron microscopy (SEM). The physicochemical properties of the cerium oxide nanoparticles were examined using XRD, which supported their crystalline nature. Cerium oxide nanoparticles' strong efficacy against the foodborne pathogens P. aeruginosa and S. typhi, while showing reduced activity against E. aerogens, was shown in a study on the antibacterial activity of cerium oxide nanoparticles. Cerium oxide nanoparticles are attracting a great deal of attention as new nano products in the field of nanomedicine due to their distinctive properties and obvious therapeutic promise in treating a variety of illnesses.

## References


[1] M. Ghiasi, A. Malekzadeh, Synthesis, characterization and photocatalytic properties of lanthanum oxy-carbonate, lanthanum oxide and lanthanum hydroxide nanoparticles, Superlattices and Microstructures, 77 (2015) 295-304. https://doi.org/10.1016/j.spmi.2014.09.027

[2] K.C. Taylor. J.R. Anderson, M. Boudart (Eds.), (1984) Catalysis Science and Technology, Springer-Verlag, Berlin, 5 120-123.

[3] Commission Recommendation on the definition of nanomaterial (Text with EEA relevance)(2011/696/EU) Journal of the European Union (2011). https://eur-lex.europa.eu/eli/reco/2011/696/oj

[4] A. Arumugam, C. Karthikeyan, A.S. Haja Hameed, K. Gopinath, S. Gowri, V. Karthika, Synthesis of cerium oxide nanoparticles using Gloriosa superba L. leaf extract and their structural, optical and antibacterial properties, Materials Science and Engineering: C, 49 (2015) 408-415. https://doi.org/10.1016/j.msec.2015.01.042

[5] M.A. Dar, R. Gul, P. Karuppiah, N.A. Al-Dhabi, A.A. Alfadda, Antibacterial Activity of Cerium Oxide Nanoparticles against ESKAPE Pathogens, Crystals, 12(2) 2022 179. https://doi.org/10.3390/cryst12020179

[6] J. Raczkowska, Y. Stetsyshyn, K. Awsiuk, M. Brzychczy-Włoch, T. Gosiewski, B. Jany, O. Lishchynskyi, Y. Shymborska, S. Nastyshyn, A. Bernasik, H. Ohar, F. Krok, D. Ochońska, A. Kostruba, A. Budkowski, “Command” surfaces with thermo-switchable antibacterial, Materials Science and Engineering: C, 103 (2019) 109806. https://doi.org/10.1016/j.msec.2019.109806

[7] S. Atiq, S.A. Siddiqi, F. Abbas, M. Saleem, S.M. Ramay, Carriers-assisted Enhanced Ferromagnetism in Al-doped ZnMnO Nano-crystallites, Chinese Journal of Chemical Physics, 26 (2013) 457-461. https://doi.org/10.1063/1674-0068/26/04/457-461

[8] G. Killivalavan, B. Sathyaseelan, G. Kavitha, I. Baskarann, K. Senthilnathan, D. Sivakumar, N. Karthikeyan, E. Manikandan, M. Maaza, Cobalt Metal ion Doped Cerium Oxide ($CoCeO_2$) Nanoparticles Effect Enhanced Photocatalytic Activity, MRS Advances, 5 (2020) 2503–2515 https://doi.org/10.1557/adv.2020.296

[9] H.A. Alshaikhi, A.M. Asiri, K.A. Alamry, H.M. Marwani, S.Y. Alfifi, S.B. Khan, Copper

Nanoparticles Decorated Alginate/Cobalt-Doped Cerium Oxide Composite Beads for Catalytic Reduction and Photodegradation of Organic Dyes, Polymers, 14(20) (2022) 4458. https://doi.org/10.3390/polym14204458

[10] M. Darroudi, M. Sarani, R.K. Oskuee, A.K. Zak, H.A. Hosseini, L. Gholami, Green synthesis and evaluation of metabolic activity of starch mediated nanoceria, Ceramics International, 40(1) B (2014) 2041-2045. https://doi.org/10.1016/j.ceramint.2013.07.116

[11] P.B. Devaraja, D.N. Avadhani, S.C. Prashantha, H. Nagabhushana, S.C. Sharma, B.M. Nagabhushana, H.P. Nagaswarupa, H.B. Premkumar, MgO:$Eu^{3+}$ red nanophosphor: Low temperature synthesis and photoluminescence properties, Spectrochimica Acta Part A: Molecular and Biomolecular Spectroscopy, 121 (2014) 46-52. https://doi.org/10.1016/j.saa.2013.10.060

[12] N. Dhananjaya, H. Nagabhushana, B.M. Nagabhushana, B. Rudraswamy, S.C. Sharma, D.V. Sunitha, C. Shivakumara, R.P.S. Chakradhar, Effect of different fuels on structural, thermo and photoluminescent properties of $Gd_2O_3$ nanoparticles, Spectrochimica Acta Part A: Molecular and Biomolecular Spectroscopy, 96 (2012) 532-540. https://doi.org/10.1016/j.saa.2012.04.067

[13] E-I Negishi, G. Wang, H. Rao, Z. Xu, Alkyne Elementometalation−Pd-Catalyzed Cross-Coupling Toward Synthesis of All Conceivable Types of Acyclic Alkenes in High Yields, Efficiently, Selectively, Economically, and Safely: "Green" Way, The Journal of Organic Chemistry, 75(10) (2010) 3151-3182. https://doi.org/10.1021/jo1003218

[14] J.M.D. Coey, A.P. Douvalis, C.B. Fitzgerald, M.Venkatesan, Ferromagnetism in Fe-doped $SnO_2$ thin films, Applied Physics Letters, 84(8) (2004) 1332–1334. https://doi.org/10.1063/1.1650041

[15] M.Y. Ge, H. Wang, E.Z. Liu, J.F. Liu, J.Z. Jiang, Y.K. Li, Z.A. Xu, H.Y. Li,On the origin of ferromagnetism in $CeO_2$ nanocubes, Applied Physics Letters, 93 (2008) 062505. https://doi.org/10.1063/1.2972118

[16] S. Atiq, S.A. Siddiqi, F. Abbas, M. Saleem, S.M. Ramay, Carrier-assisted enhanced ferromagnetism in Al-doped ZnMnO Nano-crystallites, Chinese Journal of Chemical Physics, 26(2013) 457- 461. https://doi.org/10.1063/1674-0068/26/04/457-461

[17] S. Kumar, Y.J. Kim, B.H. Koo, H. Choi, C.G. Lee, Structural and Magnetic Properties of Co Doped CeO2 Nano-Particles, IEEE Transactions on Magnetics, 45(6) (2009) 2439-2441. https://doi.org/10.1109/TMAG.2009.2018602

[18] V. Fernandes, J.J. Klein, N. Mattoso, D.H. Mosca, E. Silveira, E. Ribeiro, W.H. Schreiner, J. Varalda, A.J.A. de Oliveira, Room temperature ferromagnetism in Co-doped $CeO_2$films on Si(001) Physical Review B, 75(2007) 121304-121309. https://doi.org/10.1103/PhysRevB.75.121304

[19] L.M. Wagner, M.K. Danks, New therapeutic targets for the treatment of high-risk neuroblastoma, Journal of Cellular Biochemistry, 107(2009) 46-57. https://doi.org/10.1002/jcb.22094

[20] M. Volmer, J. Neamtu, Magnetic field sensors based on Permalloy multilayers and nanogranular films, Journal of Magnetism and Magnetic Materials, 316(2) (2014) e265-e268. https://doi.org/10.1016/j.jmmm.2007.02.115

[21] A. Lateef, S.M. Oladejo, P.O. Akinola, D.A. Aina, L.S. Beukes, B.I. Folarin, E.B. Gueguim-Kana, Facile synthesis of silver nanoparticles using leaf extract of Hyptis suaveolens (L.) Poit for environmental and biomedical applications, IOP Conference Series: Materials Science and Engineering, 805 (2020) 012042. https://doi.org/10.1088/1757-899X/805/1/012042

[22] P. Kanmani, S.T.Lim, Synthesis and structural characterization of silver nanoparticles using bacterial exopolysaccharide and its antimicrobial activity against food and multidrug resistant pathogens, Process Biochemistry, 48(7) (2013) 1099-1106. https://doi.org/10.1016/j.procbio.2013.05.011

[23] S. Malathi, K. Jagathy, A. Ram Kumar, S. Selvaraj, An In Vivo Synergistic Research on the Assessment of the Phytocompound Capped Silver Nanoparticles from Raphanus sativus Leaf Extract and Curcuma longa Against UTI-Causing E.coli., Physical Chemistry Research, 10(4) (2022) 581-588.

[24] M. Mani, R. Harikrishnan, P. Purushothaman, S. Pavithra, P. Rajkumar, S. Kumaresan, D.A. Al Farraj, M.S. Elshikh, B.Balasubramanian, K. Kaviyarasu, Systematic green synthesis of silver oxide nanoparticles for antimicrobial activity, Environmental Research, 202 (2021) 111627. https://doi.org/10.1016/j.envres.2021.111627

[25] P. Maleki, F. Nemati, A. Gholoobi, A. Hashemzadeh, Z. Sabouri, M. Darroudi, Green facile synthesis of silver-doped cerium oxide nanoparticles and investigation of their cytotoxicity and antibacterial activity, Inorganic Chemistry Communications, 131 (2021) 107682. https://doi.org/10.1016/j.inoche.2021.108762

[26] I.A. Farias, C.C. Santos, F.C. Sampaio, Antimicrobial Activity of Cerium Oxide Nanoparticles on Opportunistic Microorganisms: A Systematic Review, BioMed Research International, 1923606 (2018) 1-14. https://doi.org/10.1155/2018/1923606

[27] R. Suresh, A. Yogeshwaran, P. Logababu, P.S. Sharath, G. Aakash, V. Pugazhendhi, Empowerment the antibacterial activity of Silver Oxide nanoparticles using Woodfordia Fruticosa flower extract, International Research Journal of Multidisciplinary Technovation, 5(4) (2023) 1-11. https://doi.org/10.54392/irjmt2341

[28] H.H. Lara, N.V. Ayala-Núñez, L.C.I. Turrent, C.R. Padilla, Bactericidal effect of silver nanoparticles against multidrug-resistant bacteria, World Journal of Microbiology and Biotechnology, 26 (2010) 615–621. https://doi.org/10.1007/s11274-009-0211-3

[29] I. Sondi, O. Siiman, E. Matijević, Synthesis of CdSe nanoparticles in the presence of aminodextran as stabilizing and capping agent, Journal of Colloid and Interface Science, 275(2) (2004) 503-507. https://doi.org/10.1016/j.jcis.2004.02.005

[30] M.P. Nikolova, M.S. Chavali, Metal Oxide Nanoparticles as Biomedical Materials. Biomimetics. 2020; 5(2):27. https://doi.org/10.3390/biomimetics5020027

[31] Clinical and Laboratory Standards Institute (CLSI). Performance Standards for Antimicrobial Susceptibility Testing, 30th ed.; CLSI Supplement M100; Clinical and Laboratory Standards Institute: Wayne, PA, USA, 2020. https://clsi.org/media/3481/m100ed30_sample.pdf

[32] H.A. Hemeg, Nanomaterials for alternative antibacterial therapy, International Journal of Nanomedicine, 12 (2017) 8211–8225. https://doi.org/10.2147/IJN.S132163

[33] M. Mani, M.K. Okla, S. Selvaraj, A. Ram Kumar, S. Kumaresan, A. Muthukumaran, K. Kaviyarasu, M.A. El-Tayeb, Y.B. Elbadawi, K.S. Almaary, B.M.A. Almunqedhi, A novel biogenic Allium cepa leaf mediated silver nanoparticles for antimicrobial, antioxidant, and anticancer effects on MCF-7 cellline, Environmental Research, 198 (2021) 111199. https://doi.org/10.1016/j.envres.2021.111199

## Has this article screened for similarity?

Yes

## Acknowledgment

The author (C. Kumaran) would like to thank the Principal, Head of the Department of Physics and Microbiology, and other faculties at Sri Akilandeswari Women's College, Wandiwash-604408, Tamil Nadu, India, for their invaluable support in carrying out this entire research work.

## Author Contribution Statement

**C. Kumaran:** Conceptualization, Writing – Original draft, Validation, Investigation; **I. Baskaran:** Writing – Review & Editing, Methodology, Conceptualization, Supervision; **K. Vanmathi Selvi:** Resources, Investigation, Validation, Writing – Review & Editing; **C. Senthamil Selvi:** Visualization, Conceptualization; **P. Rajkumar:** Conceptualization, Validation, Methodology; **S. Selvaraj:** Formal analysis, Data Curation, Visualization. All authors read and approved the final manuscript.

## Conflict of Interest

The Authors have no conflicts of interest on this article to declare.

## About the License